HAL
open science

Machine precision assessment for 3D/2D digital subtracted angiography images registration

Erwan Kerrien, Régis Vaillant, Laurent Launay, Marie-Odile Berger, Eric Maurincomme

To cite this version:

Erwan Kerrien, Régis Vaillant, Laurent Launay, Marie-Odile Berger, Eric Maurincomme. Machine precision assessment for 3D/2D digital subtracted angiography images registration. SPIE Medical Imaging'98, 1998, San Diego, USA, 11 p. inria-00098697

HAL Id: inria-00098697

https://inria.hal.science/inria-00098697v1

Submitted on 26 Sep 2006

HAL is a multi-disciplinary open access archive for the deposit and dissemination of scientific research documents, whether they are published or not. The documents may come from teaching and research institutions in France or abroad, or from public or private research centers.

L'archive ouverte pluridisciplinaire **HAL**, est destinée au dépôt et à la diffusion de documents scientifiques de niveau recherche, publiés ou non, émanant des établissements d'enseignement et de recherche français ou étrangers, des laboratoires publics ou privés.

Machine precision assessment for 3D/2D digital subtracted angiography images registration

Erwan Kerrien[a,b], Régis Vaillant[b], Laurent Launay[b], Marie-Odile Berger[a], Eric Maurincomme[b], and Luc Picard[c]

[a]LORIA - BP 239 - 54506 Vandœuvre lès Nancy - France

[b]GEMSE - ISD/AAP - 283, rue de la Minière - BP 34 - 78533 Buc cedex - France

[c]Diagnostic and Therapeutic Neuroradiology Dept, CHU St Julien Hospital - 1, rue Foller - 54035 Nancy cedex - France

e-mail: Erwan.Kerrien@loria.fr

Abstract

During an interventional neuroradiology exam, knowing the exact location of the catheter tip with respect to the patient can dramatically help the physician. An image registration between digital subtracted angiography (DSA) images and a volumic pre-operative image (magnetic resonance or computed tomography volumes) is a way to infer this important information. This mono-patient multimodality matching can be reduced to finding the projection matrix that transforms any voxel of the volume onto the DSA image plane. This modelization is unfortunately not valid in the case of distorted images, which is the case for DSA images.

A classical angiography room can now generate 3D X-ray angiography volumes (3DXA). Since the DSA images are obtained with the same machine, it should be possible to deduce the projection matrix from the sensor data indicating the current machine position.

We propose an interpolation scheme, associated to a pre-operative calibration of the machine that allows us to correct the distortions in the image at any position used during the exam with a precision of one pixel. Thereafter, we describe some calibration procedures and an associated model of the machine that can provide us with a projection matrix at any position of the machine.

Thus, we obtain a machine-based 2D DSA/3DXA registration. The misregistration error can be limited to 2.5 mm if the patient is well centered within the system. This error is confirmed by a validation on a phantom of the vascular tree. This validation also yields that the residual error is a translation in the 3D space.

As a consequence, the registration method presented in this paper can be used as an initial guess to an iterative refining algorithm.

Keywords: Digital Subtracted Angiography, 3D X-ray angiography, multimodality, distortion correction, camera calibration.

1 INTRODUCTION

In interventional neuroradiology, it is of highest importance that the physician knows at any moment where the catheter lies in the body of the patient with a millimetric precision. This information might be deduced from digital subtracted angiography (DSA) images that the radiologist would relate to pre-operative magnetic resonance (MR) or computed tomography (CT) images thanks to his/her anatomical knowledge.

Many studies aim at automatically performing this mono-patient, multimodality registration. The general problem is to find a rigid transformation in the case of 3D/3D registration or a projection matrix in the case of 2D/3D image matching. Three groups of solutions arise: use of external markers (stereotactic frame [6, 9]; bullets made of lead or filled with gadolinium, glued on the patient's skin [11], etc.), use of internal or anatomical markers (extraction of image primitives: points [7], curves [1, 5], surfaces [3, 6, 10] which are matched afterwards), optimization of voxel similarity measures ([2, 6, 14, 15]). Pre-processing is necessary in order to at least correct distortions that one may encounter in many medical imaging modalities (DSA [8], MR [6, 16]).

The techniques using external markers either are constraining for the patient or lack of precision, but they constitute the gold standard for image registration. The detection of internal markers requires a high level of repeatability accross different modalities but the associated algorithms are fast since they are working on a relatively small number points. Voxel similarity measures need images with a high informative content (CT, MR) but they are more robust since they consider the whole volume data. Globally, such registrations remain limited to a pre- or post-operative use.

In interventional neuroradiology, the first intra-operative multimodality action consists in attempting to locate the catheter tip within a 3-dimensional (3D) angiography image. This kind of volume has a very weak informative content since it shows only blood vessels. The information lies more in the displayed structures than in the voxels values. Registration schemes were proposed between MR angiography (MRA) and DSA that used the first two groups of methods [1, 5, 10, 11]. The CT angiography (CTA) does not carry a much better resolution than MRA but is closer to DSA, since it is also based on the injection of a contrast product which is opaque to X-rays. Today, we can build 3D X-ray angiography volumes (3DXA) from DSA images obtained with a classical angiography room.

The 3DXA/2DDSA registration problem is slightly different in the sense that both images are acquired with the same machine, and without the patient to be displaced between the two acquisitions. We studied the possibility to define a model for the machine and use it to infer a 3D/2D registration. We showed that a submillimetric precision could not be obtained and therefore this solution could not be used within a clinical application. However, we could determine the physical limits to such a required precision and highlight the important parameters to be especially looked after when designing a machine. Furthermore, the precision that such a matching brought was enough to be used as an initial guess for an iterative improvement algorithm.

1.1 Description of the angiography machine

The angiography device is a biplan angiography system LCN+ (General Electric Medical Systems). We only studied the frontal plane. We can make out three separate parts. The X-ray tube and the image intensifier (II) are gathered in the *image chain*. The tube emits X-rays that the II receives after they have gone through the patient's head. A digital image is created and sent to an image visualization digital desk. The II may be brought closer or farther from the tube, a field of view (FOV) may be chosen and the image resolution changed (512^2 or 1024^2 image matrix). The image chain is mounted on a *C-arm* in order to change the orientation of the image chain with respect to the patient. This orientation is classically described thanks to two "anatomical" angles (cranio-caudal and right-left) but is physically decomposed in three rotation axis (L, C, P; cf figure 1). Since the L angle is of little interest for interventional neuroradiology, we decided not to take it into account in our study.

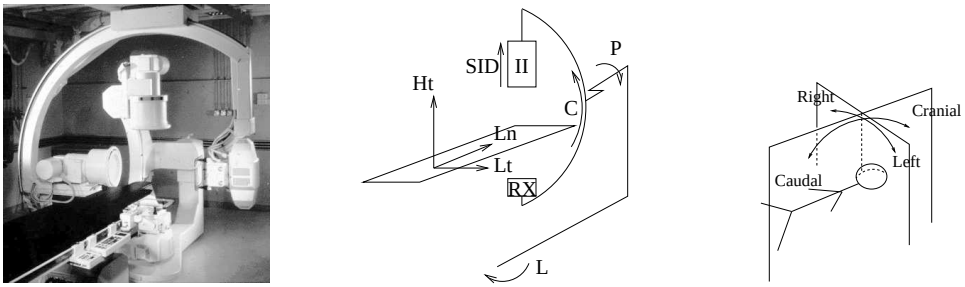

Figure 1: Angiography machine and anatomical angles

The patient lies on a *table* that may be translated along three orthogonal directions: lateral (Lt), longitudinal (Ln) and height (Ht). This machine produces DSA projective images but it may also generate 3DXA volumes. The C-arm turns at high speed around the patient's head (rotation along the P axis, called spin acquisition) while the system takes about 50 DSA images at different positions. These images are used as inputs to a tomography algorithm which builds a 3DXA volume [18]. The size of a voxel within such a volume is 0.3 mm which thus enables the physician to see arteries with an internal diameter lesser than 1 mm.

In this study, we shall only use 512^2 image matrices since 3DXA volumes are 512^3 and are based on such images. We shall consider 3 FOV dimensions: 30 cm (12 inch), 22 cm (9 inch) and 16 cm (6 inch). In these cases, if the distance between the II and the tube (source to image distance SID) is such that the magnification factor is about 1.7, an error of one millimeter will be translated in the image plane into an approximate error of (respectively): 3, 4 and 5.5 pixels.

1.2 Model of the angiography machine

We use a decomposition which is classical in vision: distortion/conic projection [12, 17]. This approach was also adopted for 3DXA [18]. A grid, formed by bars opaque to X-rays, is used in order to estimate the distortion field: at every node (intersection of two grid bars) the distortion is evaluated. The distortion field for the whole image is then determined by interpolation [8]. The conic projection is expressed thanks to a 3×4 matrix [17]. It is calibrated on a phantom (helix) designed for a 3DXA calibration [13]. Both phantoms are shown in figure 2.

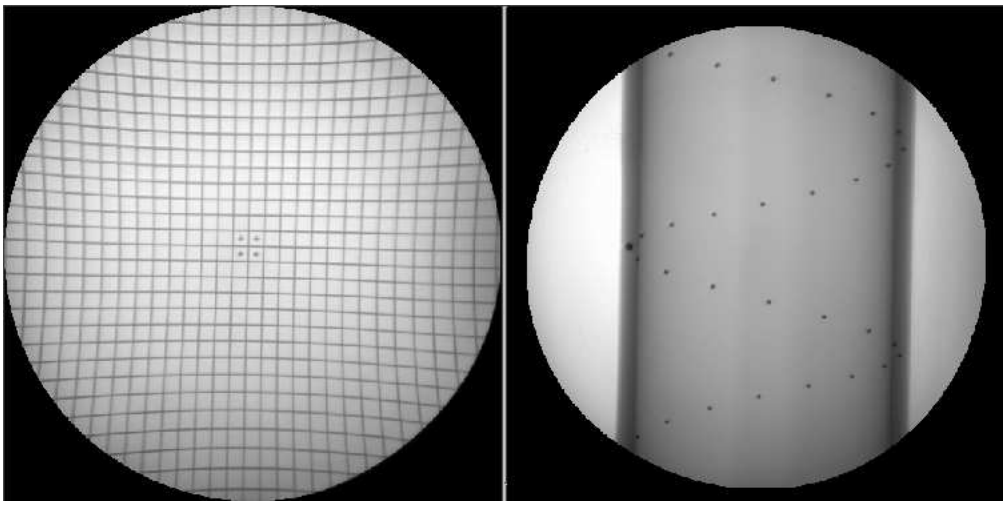

Figure 2: Distorted image of the grid and corrected image of the helix (FOV 30 cm)

The source of II distortions have been extensively studied in II physics. They mainly depend on the curvature of the entrance window and the orientation of the II with respect to the local magnetic field. Distortions must be corrected for any image chain position, with a protocol less stringent than the protocol used for stereotactic DSA exams [4]. We propose in section 2 to use the grid on a finite (small) number of positions to determine the distortion fields in these orientations before the exam begins and infer the distortion field in the current position from them during the exam.

In section 3, we describe a model of the movements of the machine which relates data given by sensors to the conic projection in the current position. As stated in the introduction, once the distortions have been corrected (pre-processing), the conic projection provides us with a 2D/3D angiography registration.

Lastly, we relate some validation made on a specific phantom and assess the precision that can be expected using such a registration method.

2 DISTORTIONS

The distortions have a variable component which depends only on the orientation of the II. As a result, they vary according to anatomical angles. If we observe grid images during a spin acquisition, we notice the distortions evolve in a slow and smooth way. We then may be able to determine them using a low degree interpolation. The estimation of the distortion field is based only on the positions of the grid nodes in the image. The interpolation will concern these positions. We call α the left-right angle and β the cranio-caudal angle. The anatomical positions the C-arm may reach is limited to $\alpha \in [-90, 90]$ and $\beta \in [-40, 40]$ in degrees.

The error we use is the Euclidian distance between the interpolated position of a node and the observed one. We can therefore calculate three different errors:

- the average error: mean of all errors for all nodes in all images
- the maximum error: maximum of all errors for all nodes in all images
- the maximum average error: maximum of the average errors calculated for each image

In order to estimate such errors, we take images of the grid at different anatomical positions. We use some of them to interpolate the other ones. The errors only take into account interpolated images.

Quadratic interpolation was chosen. Different interpolation control positions were tried out. This showed that we had to use the positions that lie on the limits of the parameter space: the quadratic interpolation using $\alpha = -90, 0, 90$ led to a maximum error of less than one pixel in 30 cm FOV. Other positions yielded errors of more than 2 pixels for images taken outside of the angular domain determined by the control points. Another constraint guided our choice: a biquadratic interpolation requires only 9 positions to be calibrated, which is already heavy within a hospital context. The control positions are thus given by the following set:

$$\{(\alpha_c, \beta_c) \text{ s. t. } \alpha_c \in \{-90, 0, 90\} \text{ and } \beta_c \in \{-40, 0, 40\}\}$$

We first performed our interpolation using a linear variation of the interpolating parameters (u, v) with respect to the variables (α, β):

$$u = \frac{\alpha + \alpha_0}{2\alpha_0} \qquad \text{et} \qquad v = \frac{\beta + \beta_0}{2\beta_0}$$

Where $\alpha_0 = 90$ and $\beta_0 = 40$. In these conditions, we were able to recover the distortion field at any anatomical position with an average error of 1.69 pixels and a maximum error of 2.11 pixels (30 cm wide FOV).

With a closer look at the grid images, it can be noticed that the evolution of the distortions is not constant. This phenomenon can be reproduced by letting the (u, v) parameters vary in a non-linear way with respect to (α, β). We can represent this non-linearity as shown in figure 3.

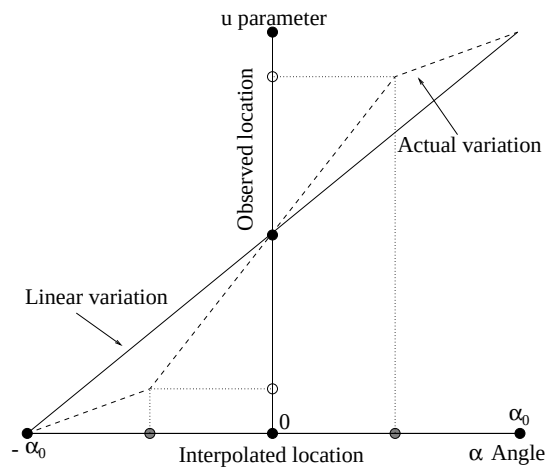

Figure 3: Non linear evolution of the interpolation parameter as a function of the angle

We defined a family of functions which depend on a parameter A, and whose evolution is close to the observed curve:

$$g_A(x) = \frac{\sin(\pi x/2A)}{\sin(\pi/2A)}$$

We did not try to relate these functions to any physical reality. If we put $u = g_A(\alpha)$ and $v = g_A(\beta)$, we obtain a dramatic improvement of the result for $A = 1.15$. This consitutes the final interpolating scheme whose performances are summarized in table 1.

The degradation of the maximal error is not alarming since it is very sensitive to noise. We conclude that geometric distortions can be recovered with a good precision (around one pixel). It is also very important to notice that it does not depend on the FOV: since the registration error should be understood in millimeters, the role of the distortion interpolation in the whole registration error will be reduced if we work with a small FOV.

FOV	E_0 30	E_0 22	E_0 16	E_4 30	E_4 22	E_4 16
average error	0.607	0.719	0.797	0.750	0.829	0.866
average maximum error	1.103	1.270	1.434	1.451	1.570	1.693
maximum error	1.566	1.685	1.992	2.627	3.108	3.188

Table 1: E_0 is the initial experiment: distortion calibration as indicated above, grid images taken for α between -90 and 90 degrees every 30 degrees and β between -40 and 40 degrees every 20 degrees (all combinations made). If we exclude the control positions (α_c, β_c), we obtain 26 different positions to calculate our errors. E_4 is the same experiment repeted 4 days later but we used the control positions of E_0 to interpolate the 26 positions of E_4. This enabled us to assess the stability of the method accross time. All errors are given in pixels.

3 CONIC GEOMETRY

The image chain is modeled as a camera. Once the distortions are corrected, this camera follows a perfect conic geometry which is mathematically expressed as a 3×4 projection matrix. Sensors indicate the intrinsic state and position of the image chain. We can therefore relate the data provided by the sensors to the intrinsic and extrinsic parameters of the projection matrix.

3.1 Intrinsic parameters

The distortions correction provides us with images whose pixel size is perfectly known in metric unit and whose axes are orthogonal (we perfectly know the geometry of the grid phantom). We assume that the projection of the optical center is right in the middle of the image. On the other hand, the focal distance is in fact the SID (sensor datum) plus a constant:

$$f = SID + a$$

The SID is known with a millimetric precision. The constant does not depend on the C-arm position and could therefore be calibrated a priori. We acquired many images of the helix phantom with different SID values, yielding sample values for a. The final value we chose for a was the mean of these samples (-122.46 mm). The maximum error made on this value was less than 0.5 mm.

From now on we consider we perfectly know our intrinsic parameters. The estimation of the projection matrix from a corrected image of the helix is performed via a Powell minimization over 6 parameters (only the extrinsics).

3.2 Extrinsic parameters

The extrinsic parameters describe the position of the camera in the helix-relative frame. This frame is not constant over two different calibrations (the helix might have been displaced). We consider a reference position for the C-arm: L=P=C=0. (which is equivalent to $\alpha = \beta = 0$). The frame relative to the camera in this position is called the *reference frame*. If we take an image of the helix in this position, we can determine a projection matrix which is decomposed (up to a scale factor) in intrinsic and extrinsic parameters:

$$M_0 = \mathcal{I}_0 \mathcal{E}_0$$

The extrinsics $\mathcal{E}_0$ describe the position of the camera with respect to the helix. Vice-versa, they give the position of the helix in the reference frame.

If we do not change the SID (the intrinsics are kept constant), we obtain for another position of the machine:

$$M = \mathcal{I}_0 \mathcal{E}$$

The extrinsics $\mathcal{E}$ represent the position of the camera with respect to the helix. As a consequence, the matrix:

$$D = \mathcal{E}_0^{-1} \mathcal{E}$$

is the rigid transformation, expressed in the helix-relative frame, which gives the movement of the helix with respect to the camera. It can be decomposed into table movements (the helix translates with the table) and inverse of C-arm movements (the helix does not move when the C-arm is rotated). We can now express this matrix as a composition of rotations (C-arm) and translations (table):

$$D = (R_L R_P R_C)^{-1} T_{Ht} T_{Ln} T_{Lt}$$

With R_L =Id, since we do not consider the L angle. The rotations represent the movement of the C-arm along its axis P and C. Their order of application is important. The translations give the movement of the table along its three axis: Ht, Ln and Lt. Their order of application is indifferent. We shall call a *simple move*, a movement of the table/C-arm along one of these 5 axis. We assume all simple moves are independent. If the simple move is a rotation, it is fully determined by a unit vector $\vec{v}$ and a fixed point O (axial parameters) and an angle θ (sensor datum). If the simple move is a translation, it is fully determined by a unit vector $\vec{v}$ (axial parameters) and a distance d (sensor datum).

The calibration procedure for each axis follows from this equation. Let's consider we want to calibrate the axis for a given parameter p. Given the matrix in the reference projection, we chose two symmetrical positions around the reference position: p_+ and p_-. These lead to two matrices D_+ and D_- from which we extract two sets of axial parameters, a priori knowing whether the associated simple move is a rotation or a translation. Lastly, we determine an average value for the axial parameters from these two sets.

3.3 Precision of the calibration

We assumed that the 6 simple moves were independent. To make things clearer, let's consider the example of the parameter P (rotation). Two values P_+ and P_- are fixed and the calibration of this simple move is made. In order to evaluate the precision of the calibration, we take images of the helix for P=-90 to 90 degrees every 10 degrees, which give 18 projection matrices. Forming the D matrix for each of these positions, we can determine the exact corresponding value for the P angle. The calibration does not depend on the precision of the sensors. As a consequence we can synthetize the projection matrix for any of the 18 chosen positions. Comparing the synthetic matrix with the actual one (estimated from the helix) indicates the precision of the calibration.

3.3.1 Measure of error

We need a proper way to compare two projection matrices (say M_1 and M_2): the projection error. Given a point expressed in the helix relative frame, the projection error for this point is the Euclidian distance, in the image plane, between its projection by M_1 and by M_2. This error is thus given in pixels. The projection error we consider is the maximum projection error encountered on points located in a sphere with a 10 cm wide diameter (approximatively the size of half a brain). We shall denote $E(M_1, M_2)$ the projection error between matrices M_1 and M_2.

3.3.2 Residual matrix

The D matrix should be either a perfect rotation or a perfect translation. In fact, we always have a residual translation/rotation matrix. This residue is only meaningful in the case of the P rotation. We modelled the residual translation as a screwing: translation parallel to the rotation axis and whose amplitude is proportional to the angle P. The coefficient λ for this proportion was added in the set of axial parameters for the P angle.

3.3.3 Estimating the average axial parameters

Let's consider a simple move corresponding to a parameter p ($p \in$ {P,C,Lt,Ln,Ht}) and the associated reference position p_0. Though in practice we used only two positions to perform the calibration of its axial parameters (p_+ and p_-), let's assume we have N such positions: $\{p_i\}_{i\in[1..N]}$. Each couple $(p_0, p_i)_{i\in[1..N]}$ leads to a matrix D_i (see section 3.2) from which we extract the axial parameters: $(\vec{v}_i, O_i)$ if the simple move is a rotation (we shall add λ_i for the P axis), and $\vec{v}_i$ in the case of a translation. These are samples which are used to infer a final set of axial parameters ($\overline{\vec{v}}, \overline{O}$ and/or $\overline{\lambda}$, depending on the type of the simple move). In order to do so, we tried three solutions: simple averaging, minimizing the error made on the focal point position and an iterative minimization of the projection error. We shall denote M_i the projection matrix corresponding to p_i and M_i' the projection matrix

built by considering the final average set of parameters and the value p_i of the parameter. E_i is the projection error between both these matrices ($E(M_i', M_i)$). It gives an indication of the precision of the calibration of the axial parameters.

Simple averaging: the $\vec{v}$ parameter is the normalized mean of the $\vec{v}_i$:

$$\overline{\vec{v}} = \frac{\sum_i \vec{v}_i}{||\sum_i \vec{v}_i||}$$

This is valid in the case of a translation as well as a rotation. In this latter case, we have to define the average fixed point to fully determine the rotation axis. Let $\mathcal{P}$ be the plane orthogonal to $\overline{\vec{v}}$ and going trough the origin of the frame. For each i, O_i' is the intersection of $\mathcal{P}$ with the axis defined by $\vec{v}_i$ and O_i. The final fixed point is then expressed as the mean of all O_i':

$$\overline{O} = \frac{\sum_i O_i'}{N}$$

For the P rotation, we consider the λ parameter to be such that:

$$\overline{\lambda} = \frac{\sum_i \lambda_i}{N}$$

The limitation of this method is that the above equations are not related to any error measure. As a result, the projection errors E_i could not be interpreted.

Focal point position error: we assumed the position of the camera was strongly related to the position of its optical center C. If C_i' is the optical center in M_i' and C_i is the focal point in M_i, then the error we want to minimize is the sum of the quadratic distance between these two points:

$$\text{minimize} \sum_i ||C_i' - C_i||^2$$

Minimizing this criterion leads to uniquely determined values for the axial parameters.

We do not take into account the direction of the optical axis, which fully determines (with focal point position) the position of the camera in space. The use of this criterion led to an error of 1 mm in the positioning of the optical center and 0.09 degree in the direction of the optical axis (comparing M_i to M_i' for each i). This could lead to a final projection error of 6 pixels (FOV 30). In practice, however, we find a projection error of 3.26 pixels (for the P angle). We interpreted the difference between this actual value and the theoretical one by the compensation of the error made on the optical center position by the optical axis so that the camera always looks at its target.

Iterative minimization of the projection error: we used a Powell algorithm to minimize the projection error:

$$\text{minimize } \max_i E_i$$

The projection error reached when using all N positions (18 for the P angle) is 2.80 pixels (FOV 30, P angle). Since we cannot in practice use too many positions for the calibration, we performed the same estimation using only two symmetrical positions with respect to the reference. The axial parameters such obtained implied a projection error (calculated on the N positions) of 2.88 pixels (FOV 30, P angle). Over all the simple moves, we could not expect more than 0.1 pixel improvement when using all N positions compared to only 2 positions.

As a conclusion, the iterative minimization of the projection error clearly appears better than the focal point method. The simple moves are stable enough for their axial parameters to be well estimated with only two positions. As a consequence, we used this method based on two positions.

3.3.4 Results

The projection errors due to the imprecision on the axial parameters are summarized in the following table:

Axis	P	C	Lt	Ln	Ht
projection error	2.88	2.49	0.21	0.61	0.58

For the table movements, the direction of the translation is well estimated. It is not the case for the rotations even though the observed errors correspond to about 1 mm of registration error (FOV 30 with magnification factor of 1.7).

3.4 Precision of sensor data

Finally, the precision of sensor data must be assessed. Sensor data could be inferred from the D matrix. Using the same sets of positions as for the estimation of the calibration precision, the inferred value was compared to the one given directly by the sensor. We found a maximum error of 0.5 degrees for the P and C angles. Concerning the table position, we found a 2 mm error on each axis.

An error of 0.5 degrees leads to a 2 pixels projection error. It is fairly easy to see that if we carefully put our object at the isocenter of the system (reduce the sphere diameter in the projection error calculations), this error becomes unimportant. The table however leads to 6 pixels error on each direction. We should therefore try to avoid moving the table. This can be done in most cases if the patient is well centered in the machine (pathology close to the isocenter location).

The last sensor datum is the SID. We know its value with a 1 mm uncertainty. The associated projection error is only 0.18 pixel. The intrinsic parameters are, as a result, well estimated.

3.5 Conclusion

We designed a calibration procedure for every parameter of the conic geometry of the image acquisition. The intrinsic parameters were shown to be well estimated and did not induce any meaningful misregistration error.

Concerning the extrinsic parameters, we can in some cases reach an unacceptable error on the registration. This is mainly due to the fact that sensor data for the table are given in millimeters. A rough estimation based on the observed errors implies that the C-arm should position the image chain with a precision below 1 mm. But even in this case, assuming the table position is perfectly known, that would imply a misregistration of 1 mm.

As a conclusion, if we take good care in positioning the patient right at the isocenter of the system, we might expect a maximum error of about 7 pixels in the registration process.

4 VALIDATION

Overall, we cannot reach the 1 mm precision required for our real-time location of the catheter tip during an interventional neuroradiology exam. If we take good care in centering the patient within the system, we might expect a projection error of less than 8 pixels (30 cm wide FOV): 7 pixels due to the uncertainty on the image chain location in space and 1 pixel from the distortion interpolation. This represents about 2.5 mm of 3D registration error.

This error typically lies within the convergence domain of most algorithms that would aim at iteratively improve the 2D/3D registration. Furthermore, the only validation we made up to this point is based on the helix. This bears two main limitations: we cannot infer a projection matrix from any image of the helix (because of its design), and we can only work in a 30 cm wide FOV (a smaller FOV would not show enough bullets for the projection matrix estimation to be robust). In order to validate more positions and smaller FOVs, we used a phantom of the vascular tree as shown in figure 4. Basically we compared the position of some characteristic points (intersection of rods) in the image of the phantom actually taken at a given position, and the image generated by reprojecting the 3D reconstruction of the phantom by the synthetic matrix corresponding to this position (cf figure 4). This method cannot yield such a high precision as the comparison made above directly from the helix but the aim is to verify that the image we synthetize always consitutes a good initial guess for a registration refinement algorithm.

We found a maximum error equivalent to 10 pixels in a 30 cm wide FOV. An important result from this validation is however that we never observed any noticeable error neither in rotation nor in zoom: any error could

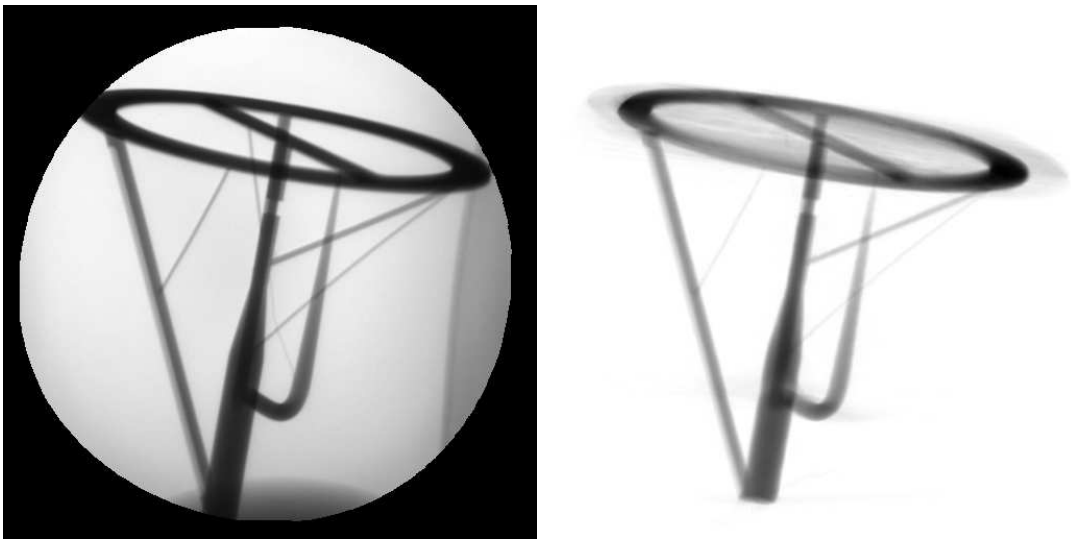

Figure 4: Image of the phantom of the vascular tree that we used (left). Synthetic image obtained by reprojection of the 3DXA reconstruction (Right). P=60, C=20, L=0, the table has not been moved, SID=1200 mm, FOV=22 cm

be corrected by tuning the table positions input for synthetizing the projection matrix. As a consequence, the rigid transformation to be estimated by a refinement algorithm in order to reach a perfect match is a simple translation: we have only 3 parameters to tune (which can be done by changing the table position).

Thanks to this validation, we have shown two important characteristics of our machine based registration: the residual error is a translation in the 3D space, and it provides an initial guess which is close to the ideal solution. Only a few iterations of an optimization algorithm acting on 3 parameters should be enough to reach a perfect match.

5 DISCUSSION

A 2D/3D registration is equivalent to the determination of a projection matrix. A distortion correction of images is done in order to validate the conic geometry hypothesis made on the acquisition system. In the case of a 2D DSA/3DXA registration, we can infer the conic geometry from sensor data indicating the current position of the angiography machine (C-arm and table), assuming that this machine has been properly calibrated. Furthermore, it is known that the II physics imply a high level of distortions in the DSA images. Such distortions are dependent on the position of the C-arm. Therefore, the distortion field cannot be a priori estimated. We propose an interpolation scheme based on a light calibration procedure to correct the distortions in any position. This scheme yields an error of approximately 1 pixel in the image plane and is stable over time.

We also described the calibration of the angiography machine, and its associated methods, which allow us to infer a 2D DSA/3DXA registration. If the patient is well centered within the system, this image matching is performed with a 2.5 mm precision. The residual error is a translation in the 3D space and could therefore be easily and rapidly corrected with an iterative refining algorithm.

We could highlight parts of the machine that should be improved in order to effectively get a better machine-based matching. However, the specifications needed to constraint the C-arm would be very challenging. Furthermore, we never took into account the fact that the patient might move between the 3D acquisition and the actual image we should want to registrate it with. As a conclusion, a refinement algorithm actually appears unavoidable.

References

[1] Alperin, N., Levin, D., and Pelizzari, C. "Retrospective registration of X-ray angiograms with MR images by using vessels as intrinsic landmarks" In *Journal of Magnetic Resonance Imaging*, volume 4, pages 139-144, 1994.

[2] Collignon, F., Maes, F, Delaere, D, Vandermeulen, D., Suetens, P, and Marchal, G. "Automated Multi-Modality Image Registration Based on Information Theory" In *Information Processing in Medical Imaging*, pages 263-274, 1995.

[3] Cuchet, E., Knoplioch, J., Dormont, D., and Marsault, C. "Registration in Neurosurgery and Neuroradiotherapy Applications" In *Journal of Image Guided Surgery*, volume 1, pages 198-207, 1995

[4] K. Ericson, M. Söderman, E. Maurincomme and C. Lindquist "Clinical Experience with Stereotactic Digital Subtraction Angiography with Distortion Correction Software" In *Journal of Stereotactic and Functional Neurosurgery*, volume 66, suppl 1, pages 63-70, 1996

[5] Jacques Feldmar and Grégoire Malandain and Nicholas Ayache and Sara Fernández-Vidal and Eric Maurincomme "Matching a 3D MR angiography volume image and 2D X-Ray angiograms" In *First International Joint Conference on Computer Vision, Virtual Reality, and Robotics in Medicine and Medical Robotics and Computer Assisted Surgery*, volume 1205, pages 129-140, March 1997

[6] Hemler, P., Van den Elsen, P., Sumanaweera, T., Napel, S., Drace, J., and Adler, J. "A quantitative comparison of residual error for three different multimodality registration techniques" In *Information Processing in Medical Imaging*, pages 251-262, 1995.

[7] Hill, D., Hawkes, D., Crossman, J., Gleeson, M., Cox, T., Bracey, E., Strong, A., and Graves, P. "Registration of MR and CT Images for Skull Base Surgery Using Point-like Anatomical Features" In *The British Journal of Radiology*, volume 64, pages 1030-1035, 1991.

[8] Launay, L., Picard, C., Maurincomme, E., Anxionnat, R., Bouchet, P., and Picard, L. "Quantitative evaluation of an algorithm for correcting geometrical distortions in dsa images: applications to stereotaxy" In *SPIE Medical Imaging*, volume 2434, pages 520-530, San Diego, 1995.

[9] Launay, L. *Localisation et reconstruction 3D à partir d'angiographies stéréotaxiques* PhD thesis, Institut National Polytechnique de Lorraine, Nancy, France, 1996.

[10] Lavallée, S., Szeliski, R., and Burnie, L. "Matching 3D Smooth Surfaces with their 2D projections Using 3D Distance Maps" In *SPIE Geometric Methods in Computer Vision*, volume 1570, pages 322-336, 1991.

[11] Masutani, Y., Furukawa, C., Sonderegger, M., Masamune, K., Suzuki, M., Dohi, T., Yamane, F., Iseki, H., and Takakura, K. "3D position visualization of catheter tip for intravascular neurosurgery using 3D structural description of vasculature" In *Computer Assisted Radiology*, pages 821-826, 1996.

[12] Peuchot, B. "Utilisation de détecteurs subpixels dans la modélisation d'une caméra" In *RFIA*, pages 691-695, 1994.

[13] Rougée, A., Picard, C., Ponchut, C., and Trousset, Y. "Geometrical calibration of X-ray imaging chains for three-dimensional reconstruction" In *Computerized Medical Imaging and Graphics*, volume 17(4/5), pages 295-300, 1993.

[14] Studholme, C., Hill, D., and Hawkes, D. "Multiresolution voxel similarity measures for MR-PET registration" In *Information Processing in Medical Imaging*, pages 287-298, 1995.

[15] Studholme, C., Hill, D., and Hawkes, D. "Automated 3D Registration of MR and CT Images of the Head" In *Medical Image Analysis*, volume 1, issue 2, March 1996.

[16] Sumanaweera, T., Glover, G., Hemler, P, Van den Elsen, P, Martin, D., Adler, J., Napel, S. "MR Geometric Distortion Correction for Improved Frame-Based Stereotactic Target Localization" In *MRM*, volume 34, pages 106-113, 1995.

[17] Toscani, G *Systèmes de calibration et perception du mouvement en vision artificielle* PhD thesis, Université de Paris-Sud, Orsay, 1987.

[18] Trousset, Y., Picard, C., Ponchut, C., Roméas, R., Campagnolo, R., Croci, S., Scarabin, J., and Amiel, M. "3D X-ray angiography: From numerical simulations to clinical routine" In *Int. Meeting on Fully 3D Image Reconstruction in Radiology and Nuclear Medicine*, pages 3-11, Aix les Bains, France, 1995.